Design and Implementation of an Institution-Wide Patient-Specific Radiation Dose Monitoring Program for Computed Tomography, Digital Radiography, and Nuclear Medicine

by

Olav Christianson

Medical Physics Graduate Program
Duke University

Date:_____

Approved:

_____
Ehsan Samei, Supervisor

_____
Robert Reiman

_____
Terry Yoshizumi

Thesis submitted in partial fulfillment of
the requirements for the degree of Master of Science in the
Medical Physics Graduate Program in the Graduate School
of Duke University

2011

ABSTRACT

Design and Implementation of an Institution-Wide Patient-Specific Radiation Dose Monitoring Program for Computed Tomography, Digital Radiography, and Nuclear Medicine

by

Olav Christianson

Medical Physics Graduate Program
Duke University

Date:_____
Approved:

_____
Ehsan Samei, Supervisor

_____
Robert Reiman

_____
Terry Yoshizumi

An abstract of a thesis submitted in partial
fulfillment of the requirements for the degree
of Master of Science in the
Medical Physics Graduate Program in the Graduate School
of Duke University

2011

Abstract

Recently, there has been renewed interest in decreasing radiation dose to patients from diagnostic imaging procedures. So far, efforts to decrease radiation dose have focused on the amount of radiation delivered from typical techniques and fail to capture the variation in radiation dose between patients. Despite the feasibility of estimating patient-specific radiation doses and the potential for this practice to aid in quality assurance, it is not currently standard procedure for hospitals to monitor radiation dose for all patients. To address this shortcoming, we have developed an institution-wide patient-specific radiation dose monitoring program for computed tomography, digital radiography, and nuclear medicine.

Contents

List of Tables

List of Figures

1. Benefits of patient-specific dose monitoring in diagnostic imaging

1.1 Background

Over the last 100 years, the overwhelming benefits of ionizing radiation have firmly established its role in diagnostic medicine. Currently, ionizing radiation is used so commonly in medical imaging that it constitutes approximately 50% of the collective radiation dose to the United Stated population[1].

Recent media outlets have highlighted some of the dangers associated with the use of ionizing radiation[2]. In response, there has been renewed interest in minimizing patient radiation doses during diagnostic procedures. While most efforts attempt to standardize radiation dose to the average patient, few capture the variability in radiation dose between patients[3]. To effectively minimize radiation dose to all patients, a system capable of monitoring patient-specific radiation dose is required.

Recently, several efforts have been made to monitor patient-specific radiation dose in diagnostic imaging[4, 5]. While these efforts focus on specific imaging modalities, we have developed an institution-wide, patient-specific radiation dose monitoring system for computed tomography, digital radiography, and nuclear medicine. In this work, we will demonstrate how to implement such a system as well as how this system can facilitate quality assurance and standardization of imaging procedures.

1.2 Implementation

Implementing a patient-specific radiation dose monitoring program requires seamless integration with current clinical operations and little human maintenance. In our system, all DICOM images are automatically forwarded from the picture archiving and communication system (PACS) to digital image and communication in medicine (DICOM) routing software, where the data are sorted and relevant dose information extracted. The dose data are then sent to a dosimetry database so that patient-specific radiation doses may be calculated. These patient-specific radiation doses are reported back to the staff as an aid to improve clinical practice.

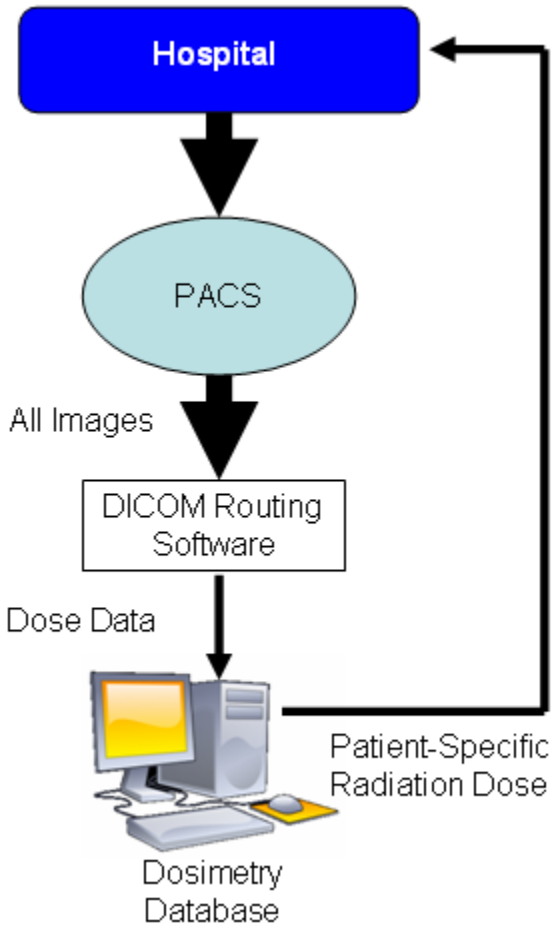

Figure 1: Schematic diagram of data flow for patient-specific dose monitoring.

To aid in the analysis of dose-related data acquired using this system, we developed graphical user interface in MATLAB capable of querying the dosimetry database. We further developed customizable data filters to isolate specific studies from the database. These filters allow us to identify studies where the patient dose exceeds diagnostic reference limits, view histograms of patient doses for specific protocols, compare patient doses between imaging equipment from multiple vendors, and generate cumulative radiation doses across all modalities. Our graphical user interface

enables us to filter the data in a meaningful way and identify ways to improve the clinical operation at our institution.

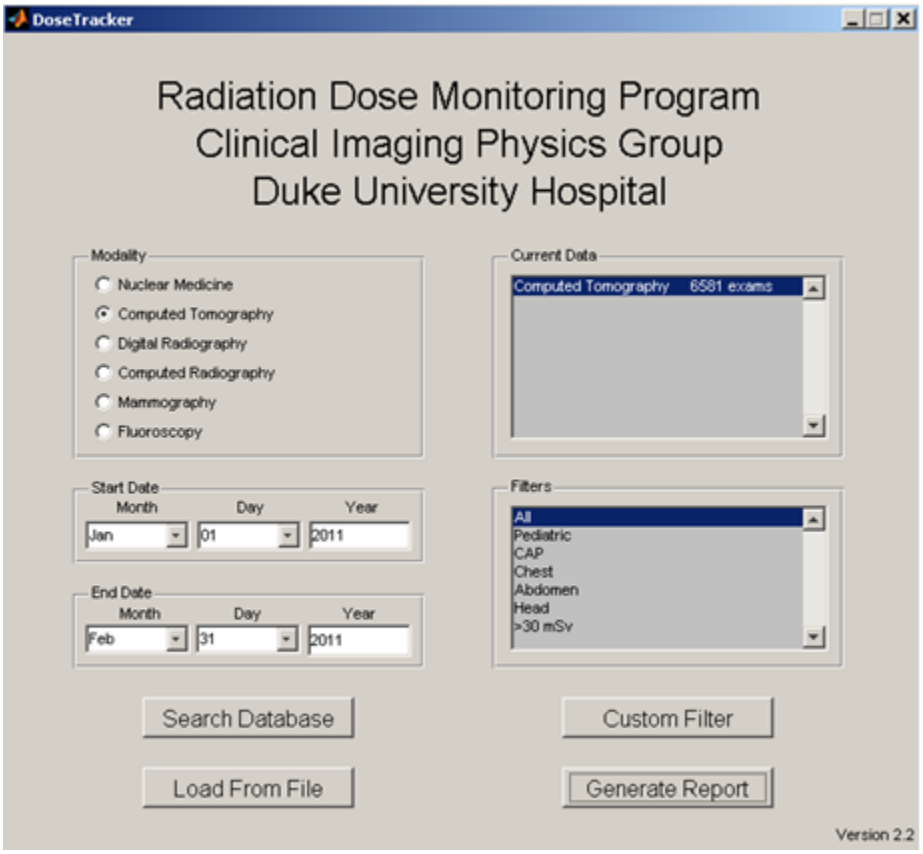

Figure 2: Graphical user interface to facilitate data analysis.

1.3 Overdose reduction

One of the primary motivations for patient-specific dose monitoring is to identify and minimize high-dose imaging procedures. To aid in this process, we employ two diagnostic levels: a reference level and an action level. The reference level, set at the 75th percentile of the patient dose distribution, is primarily used to facilitate comparison of our findings with those from previous reports. The action level, set at three times the

median patient dose for most protocols, is used to flag studies in which patients received an unexpectedly high radiation dose. All studies with patient doses in excess of the action level are flagged for review to determine the cause of the elevated dose.

1.4 Standardization

Patient doses for a given procedure vary significantly across different institutions in the United States[6, 7]. This variation in patient doses highlights the fact that some patients routinely receive more than the minimum amount of radiation necessary during their procedure. Therefore, we believe that the first step toward optimizing patient radiation doses is to standardize these doses both within and between institutions.

Past efforts at standardization have attempted to compare the radiation dose received from a typical procedure across institutions[8]. Because patient doses vary significantly even within an institution, however, this approach fails to capture inter-institutional differences in radiation dose. A better method of standardization involves comparing estimates of patient-specific doses between institutions. This method of comparison considers not only the radiation dose from the typical protocol but also the dose distribution and extremes.

1.5 Limitations

Despite the evident utility of patient-specific radiation dose monitoring, there are limits to its application. The dose calculation process relies on mathematical phantoms to model the human body. While it is not practical to customize phantoms to model

each patient's specific anatomy, using a generic phantom for all patients - even if total patient size is taken into account - introduces uncertainty into the dose calculation. Because of this concern, we will only be able to provide patient-specific estimates of radiation dose until a solution that accounts for differences in patient size and shape is presented. In spite of this limitation, patient-specific dose estimates allow identification of high-dose studies and standardization of imaging protocols.

1.6 Conclusions

Patient-specific radiation dose monitoring is necessary to minimize radiation doses to all patients. Our automated system does not interfere with clinical operations and necessitates little human maintenance. We utilize diagnostic reference levels that allow high-dose studies to be flagged and reviewed to determine the cause of elevated radiation doses, thereby preventing future overdoses. The data we obtain on patient-specific radiation doses also makes possible the accurate assessment and standardization of radiation doses across institutions. This practice improves the quality of care delivered to all patients undergoing diagnostic imaging procedures.

2. Automated patient-specific dose monitoring system for digital radiography

2.1 Background

With over two billon examinations performed annually, conventional x-ray examinations make up the largest fraction of medical imaging procedures of any imaging modality[9]. While conventional x-ray imaging uses lower radiation doses than other imaging modalities (e.g., fluoroscopy, computed tomography), it is performed so frequently that it constitutes a significant portion of the background radiation exposure to the United States population[1].

Recently, there has been renewed interest in minimizing patient radiation exposure from diagnostic imaging procedures, including conventional radiography. Because most efforts seek to optimize imaging protocols for only the average patient[3], however, current endeavors fail to capture the variability in dose between patients. Effectively minimizing patient radiation exposure thus requires a system that can efficiently monitor patient-specific radiation doses. While previous efforts have sought to establish patient-specific radiation dose monitoring programs for conventional x-ray examinations, such systems have not yet been widely adopted[10].

Digital radiography (DR) offers an intriguing platform on which to implement a patient-specific dose monitoring program. Because the kilo-voltage peak (kVp), current-time product (in units of mAs), and source-to-image distance (SID) are recorded in the Digital Image and Communication in Medicine (DICOM) headers during digital

radiography examinations, the entrance skin exposure (ESE) for a study can be calculated directly. Accordingly, numerous reports have tabulated dose conversion coefficients (DCCs) that translate ESEs into organ radiation doses[11-14]. Despite the extensive tabulation of organ DCCs, however, the lack of DCCs specific to different x-ray beam geometries and energy spectra makes application of these values across a broad range of studies difficult.

For these reasons, we sought to generate DCC tables for beam geometries of interest and clinically relevant energy spectra using Monte Carlo simulations. To facilitate the modeling of clinical energy spectra, we also determined a relationship between the half-value layer (HVL) and total filtration. Finally, we applied these DCC tables clinically to determine patient-specific radiation doses from chest DR examinations.

2.2 Methods

2.2.1 Monte Carlo-based dose conversion coefficients

DCCs were generated via PCXMC 2.0, a Monte Carlo program used for the simulation of external medial x-ray examinations[15]. Anatomical phantoms based on the mathematical models of Cristy and Eckerman[16, 17] were used along with PCXMC's ability to modify the basic phantom's height and weight. The DCCs generated using PCXMC have previously been shown to agree well with those generated from other phantom models[18, 19].

2.2.1.1 Effect of energy spectrum on DCCs

In PCXMC, the input energy spectrum is defined by three quantities: anode tube angle, kVp, and filtration in the beam. We assumed an anode tube angle of 16 degrees for all simulations, along with varied kVp (from 60 to 150 kVp) and total filtration (from 1 to 8 mm of aluminum). With this method, we were able to generate tables of DCCs for clinically relevant energy spectra using the reference phantom (178.6 cm, 73.2 kg).

2.2.1.2 Effect of patient size on DCCs

To explore the effects of patient size on effective dose (ICRP 103) DCCs, we simulated chest posterior-anterior (PA) and lateral exposures for a broad range of patient weights (50 to 150 kg) with a single energy spectrum (16 degree anode angle, 120 kVp, and 3.6 mm aluminum). We normalized the weight-specific DCCs to the reference phantom (73.2 kg) DCCs to obtain a series of correction factors. These correction factors improve accuracy of dose estimates when patient weights are known.

2.2.2 Relationship between total filtration and HVL

Simulation of energy spectra in PCXMC requires that the amount of filtration used in the x-ray beam be known. In practice, however, it is difficult to determine the composition and thickness of all materials in the x-ray beam. A commonly performed surrogate to measuring the spectrum exiting an x-ray tube is to measure the half-value layer (HVL). Due to the relative ease of obtaining HVL measurements, we developed a relationship between the HVL and total filtration.

The clinical method for measuring the HVL is a two-step process. First, the open-beam exposure is measured using an ion-chamber or other radiation measurement device. Then, the thickness of an aluminum shield between the x-ray source and the measurement device is increased incrementally until the open-beam exposure has been reduced to half of its original value. The HVL can then be calculated using the following equation:

$$HVL = \frac{\left(t_b \times \ln\left(2\frac{E_a}{E_0} \right) - t_a \times \ln\left(2\frac{E_b}{E_0} \right) \right)}{\ln\left(\frac{E_a}{E_b} \right)} \qquad (1)$$

Where E_0 is the open beam exposure, E_a is an exposure that is lower than $E_0/2$ with thickness of aluminum t_a, and E_b is an exposure that is lower than $E_0/2$ with thickness of aluminum t_b.

We duplicated this experimental design using Xspect[20], a semi-empirical modeling program for the production, attenuation, and detection of x-ray spectra. The open-beam exposure was simulated with varying amounts of inherent filtration in place. We simulated further exposure measurements, each with an additional 1 mm of aluminum attenuating the x-ray beam, until the exposure measurement was reduced to half of its original value. The HVL was calculated for each filtration setup according to equation 1. We generated curves of HVL vs. filtration for three commonly used kVps (70 kVp, 90 kVp, and 120 kVp).

2.2.3 Clinical application

All DR studies were sent through DICOM routing software. From the DICOM headers, we were able to extract the following dose-relevant information: the x-ray tube used, kVp, current-time product, SID, and imaging protocol. Since patient heights and weights were not readily available, we assumed a reference height of 178.6 cm and weight of 73.2 kg. The dose data were sent to a secure dosimetry database for further processing.

Organ and effective dose estimation consisted of several steps summarized in Figure 3. The entrance skin exposure (ESE) was obtained from the measured radiation tube output at a kVp, SID, and current-time product. The DCC was then determined from the ESE, HVL, kVp, and our DCC tables. If the kVp or total filtration did not precisely match simulated values in the DCC tables, a linear interpolation was used to approximate the actual DCC. The entrance skin exposure was then multiplied by the DCC to estimate the organ and effective dose values.

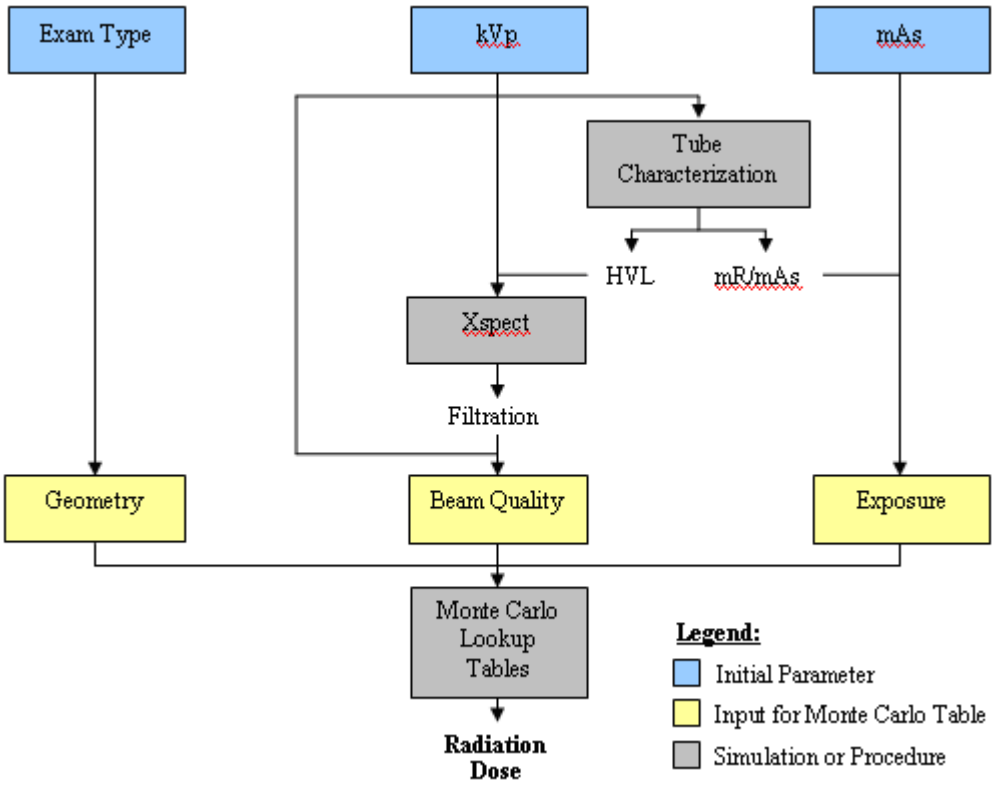

Figure 3: Diagram of the dose estimation process for DR examinations.

We collected data on 796 chest DR examinations (470 lateral projections and 326 PA projections). We limited our analysis to those cases where no additional filtration was specified in the DICOM headers.

Data analysis was complicated by the fact that not all x-ray tubes were fully characterized. We therefore developed an average x-ray tube characterization, generated by averaging the values from five known x-ray tubes, for use where data on an x-ray tube were not available. The average x-ray tube used a HVL of 3.6 mm of aluminum and the radiation output function shown in Figure 4.

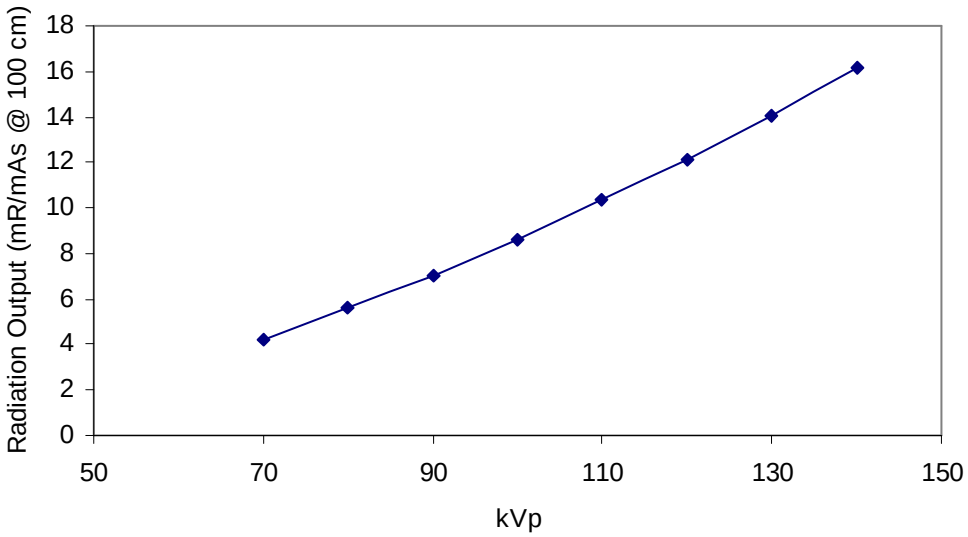

Figure 4: Radiation output for the average x-ray tube at our institution.

2.3 Results

2.3.1 Monte Carlo-based dose conversion coefficients

2.3.1.1 Effect of energy spectrum on DCCs

We generated effective dose and organ-specific DCC tables for typical x-ray examinations with a reference phantom (178.6 cm, 73.2 kg). Because chest examinations are the most common x-ray procedures, we focused our analysis on the DCCs for PA and lateral chest examinations shown in tables 1 and 2. As expected, we found that the effective dose DCCs increased with both the kVp and filtration (Figure 6). In contrast to previous reports suggesting that a single conversion factor is sufficient for all energy spectra[10], we found that the effective dose DCCs varied by as much as 50% between different clinically relevant energy spectra.

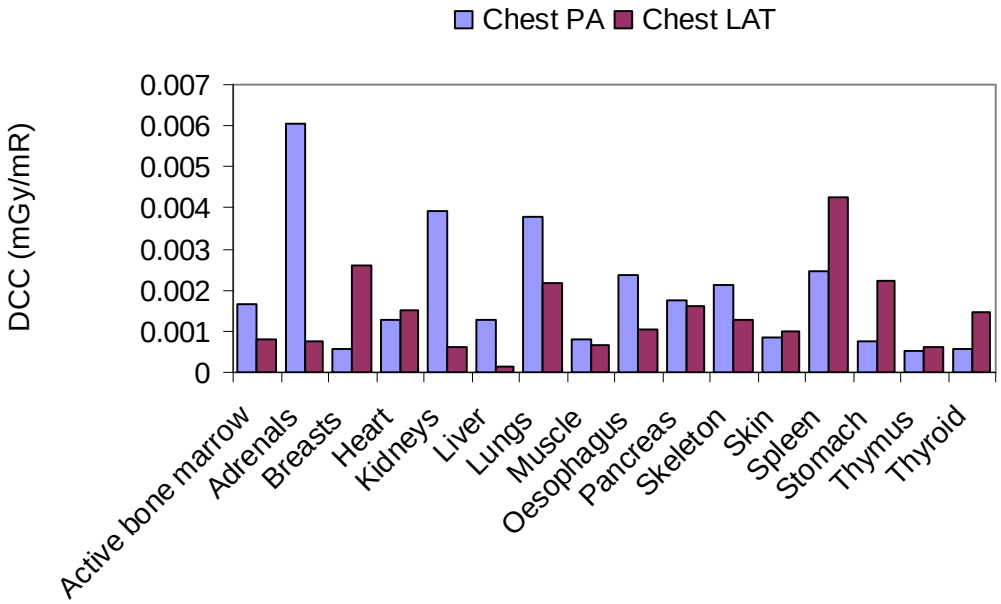

Figure 5: Organ DCCs for chest DR examinations at 120 kVp.

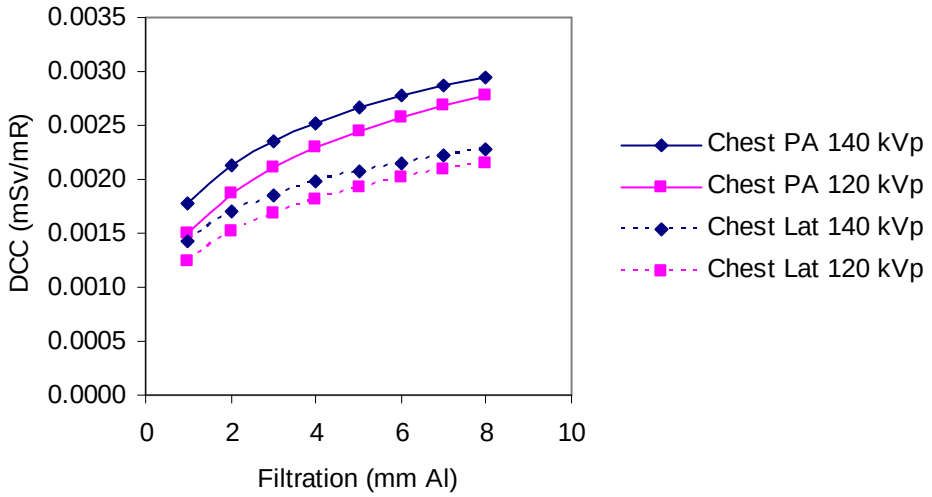

Figure 6: Effective dose DCCs for chest DR examinations.

Table 1: Effective dose DCCs (mSv/mR) for chest PA projection.

	Total filtration (mm Al)							
kVp	1	2	3	4	5	6	7	8
40	0.00025	0.00038	0.00047	0.00054	0.00061	0.00066	0.00071	0.00075
50	0.00040	0.00059	0.00074	0.00085	0.00095	0.00104	0.00111	0.00118
60	0.00055	0.00080	0.00098	0.00113	0.00126	0.00137	0.00146	0.00154
70	0.00071	0.00100	0.00121	0.00138	0.00152	0.00164	0.00175	0.00185
80	0.00087	0.00120	0.00143	0.00162	0.00177	0.00190	0.00202	0.00212
90	0.00104	0.00139	0.00163	0.00183	0.00199	0.00212	0.00224	0.00234
100	0.00120	0.00156	0.00181	0.00201	0.00217	0.00230	0.00242	0.00252
110	0.00136	0.00172	0.00197	0.00216	0.00232	0.00245	0.00256	0.00266
120	0.00151	0.00187	0.00211	0.00230	0.00245	0.00257	0.00268	0.00277
130	0.00165	0.00200	0.00224	0.00242	0.00256	0.00268	0.00278	0.00287
140	0.00178	0.00213	0.00235	0.00252	0.00266	0.00277	0.00287	0.00295
150	0.00190	0.00224	0.00245	0.00262	0.00274	0.00285	0.00294	0.00301

Table 2: Effective dose DCCs (mSv/mR) for chest lateral projection.

	Total filtration (mm Al)							
kVp	1	2	3	4	5	6	7	8
40	0.00030	0.00042	0.00051	0.00058	0.00063	0.00068	0.00072	0.00075
50	0.00042	0.00060	0.00072	0.00081	0.00089	0.00095	0.00101	0.00106
60	0.00054	0.00075	0.00090	0.00101	0.00110	0.00118	0.00125	0.00131
70	0.00066	0.00089	0.00105	0.00118	0.00129	0.00138	0.00145	0.00152
80	0.00078	0.00104	0.00121	0.00135	0.00146	0.00156	0.00164	0.00171
90	0.00090	0.00117	0.00136	0.00150	0.00161	0.00171	0.00179	0.00186
100	0.00102	0.00130	0.00148	0.00162	0.00174	0.00183	0.00191	0.00198
110	0.00114	0.00141	0.00159	0.00173	0.00184	0.00193	0.00201	0.00208
120	0.00124	0.00151	0.00169	0.00182	0.00193	0.00202	0.00209	0.00215
130	0.00134	0.00161	0.00178	0.00191	0.00201	0.00209	0.00216	0.00222
140	0.00144	0.00170	0.00186	0.00198	0.00208	0.00215	0.00222	0.00228
150	0.00152	0.00177	0.00193	0.00205	0.00214	0.00221	0.00227	0.00232

2.3.1.2 Effect of phantom size on DCCs

To determine the effect of phantom size on effective dose DCCs for chest projections, we calculated effective dose DCCs across a broad range of phantom weights (50 kg to 150 kg). We generated a series of correction factors by normalizing the DCCs

for each phantom weight to the DCCs for the reference phantom weight. As expected, the normalized DCCs exhibited an inverse relationship with phantom weight (Figure 7). The maximum deviation from the reference phantom DCCs was 46% corresponding to the heaviest phantom. The similarity between the correction factors for the two projections indicates that they can be described by a single equation.

$$C = 1.5419 \times e^{(-0.0056 \times W)} \qquad (2)$$

Where C is the correction factor and W is the patient's weight in kg.

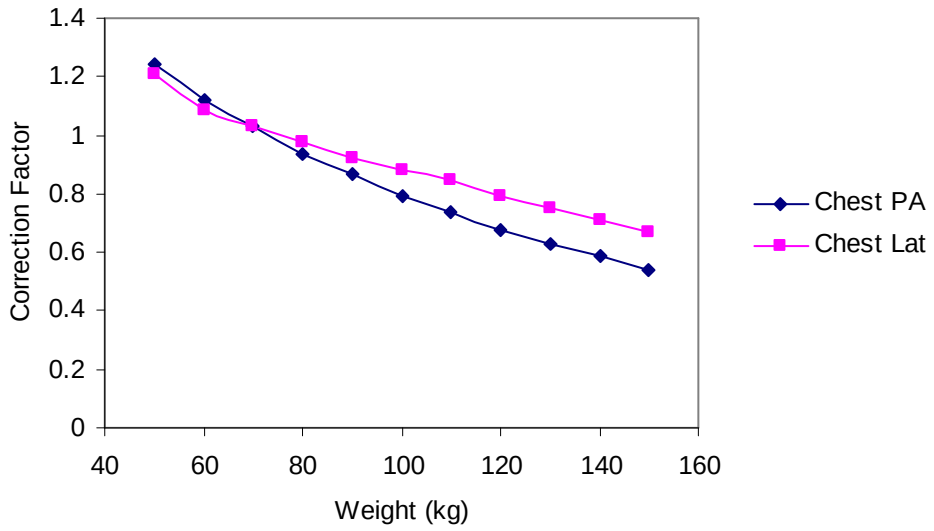

Figure 7: Patient weight DCC correction factors.

2.3.2 Relationship between HVL and total filtration

To facilitate the clinical use of our DCC tables, we developed a relationship between HVL and total filtration shown in Figure 8. For all peak energy values, there

was a quadratic relationship between the HVL and total filtration (R^2=0.9995). The relationships between HVL and total filtration are described by Equations 3-5.

70 kVp: $$filtration = 0.401 \times HVL^2 + 0.251 \times HVL - 0.034 \quad (3)$$

90 kVp: $$filtration = 0.239 \times HVL^2 + 0.263 \times HVL - 0.067 \quad (4)$$

120 kVp: $$filtration = 0.165 \times HVL^2 + 0.085 \times HVL - 0.002 \quad (5)$$

It is interesting to note that if the HVL is known at one peak energy, an approximation of the HVL can be obtained at a different peak energy by multiplying the known HVL by the ratio of the kVps. Accurate to approximately 10%, it is possible to use our model to obtain the total filtration for HVLs measured at any arbitrary peak energy.

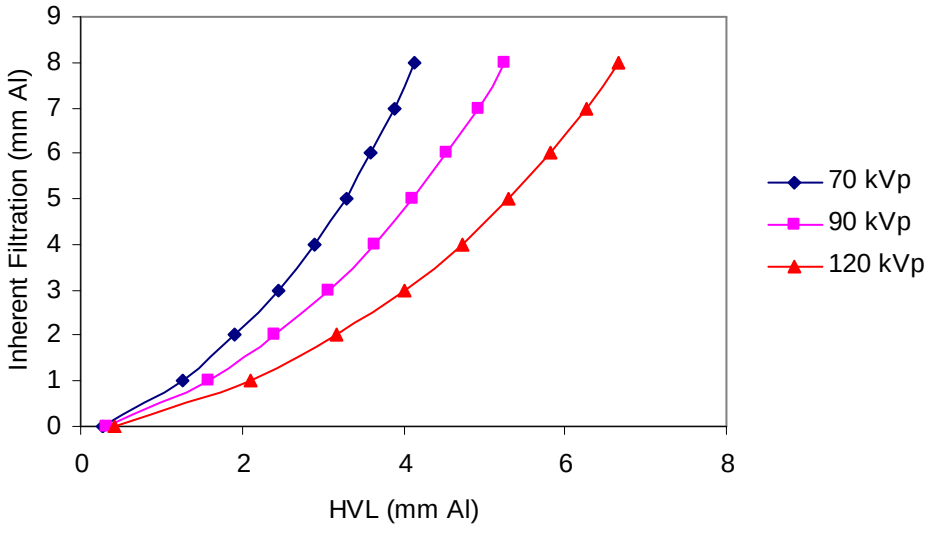

Figure 8: Total filtration vs. HVL.

2.3.3 Clinical application

To demonstrate the applicability of our method in a clinical environment, we applied our DCC tables to 796 chest DR examinations (326 PA projections and 470 lateral projections). The median patient doses were 0.028 mSv and 0.130 mSv for the PA and lateral projections, respectively. In addition to having higher doses, the distribution of patient doses for the lateral projection was much broader than that for the PA projection. As a whole, the patient doses were found to be lower than the values reported previously[3].

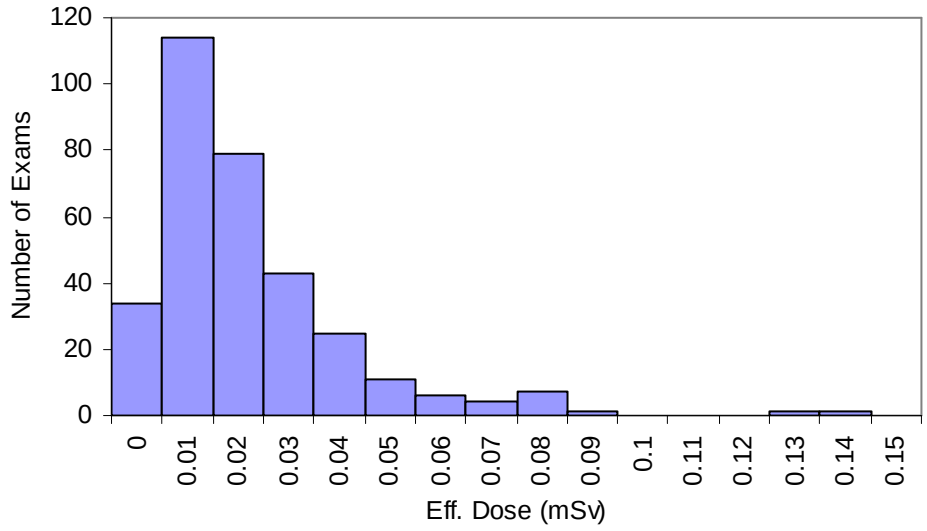

Figure 9: Histogram of patient doses from chest PA examinations.

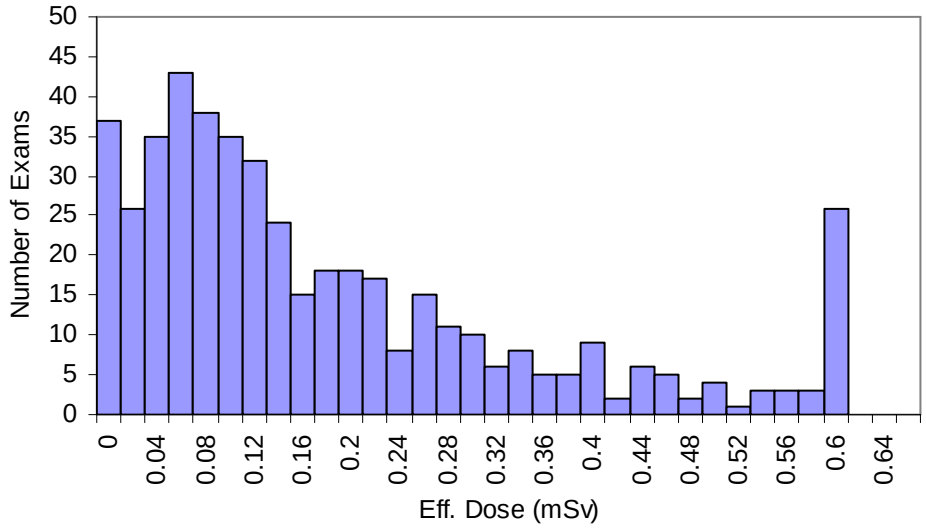

Figure 10: Histogram of patient doses from chest lateral examinations.

2.4 Discussion

To improve the quality assurance program in digital radiography, we developed a method for calculating patient-specific radiation dose from DR examinations. We generated DCC tables for all clinically relevant energy spectra based on kVp and total filtration values. To enable to use of these DCC tables with information available during normal clinical practice, we developed a method that uses the HVL to determine total filtration. Finally, we demonstrated how these DCC tables can be used clinically to calculate radiation doses in chest radiography examinations.

2.4.1 Monte Carlo-based dose conversion coefficients

We developed tabulated DCCs for typical clinical protocols using a reference phantom (178.6 cm, 73.2 kg). These tables apply to a broad range of energy spectra

defined by the filtration and kVp, allowing for their use in a wide variety of clinical situations. Further, we explored the effect of phantom size on DCCs and found a maximum deviation of 46%. We therefore developed a series of correction factors to improve precision of DCCs where patient weights are known. These correction factors can be easily adapted for use at other institutions.

The anatomical phantoms used by PCXMC to generate the DCC tables are relatively simplistic in design. More complex phantoms that resemble the human body with greater precision have recently become available for use in Monte Carlo simulations[21]. These phantoms clearly improve the accuracy of Monte Carlo simulations for single patients, but they do not greatly enhance the applicability of a phantom to the general patient population. The greatest benefit of these improved mathematical phantoms is the fact that they offer the ability to explore the effects of differences in patient size on DCCs with improved precision. For our applications, a simple phantom design has as much applicability as more complex versions.

2.4.2 Relationship between total filtration and HVL

Because the data on total filtration necessary to determine the above DCCs is not readily available during clinical imaging, we developed a simple but robust method for converting between HVL and total filtration values. To facilitate the adaptation of our method, we also demonstrated that HVL values measured at any energy spectrum can be converted to those used in this report.

While our method is simple and robust, it does have limitations. We assumed that there was a one-to-one correspondence between an x-ray tube and its equivalent total filtration of aluminum. The x-ray tube housing, however, is actually made up of several materials (e.g., silicon, oil, aluminum) that each have different attenuation profiles. In reality, it is expected that the total filtration of the housing will be equivalent to different thicknesses of aluminum when operated at different kVps. Preliminary exploration revealed that there indeed was a small difference in total filtration when our x-ray tubes were operated at different kVps. The resulting variation in effective dose DCCs, however, was negligible in comparison to other uncertainties intrinsic to patient-specific dosimetry.

2.4.3 Clinical application

We demonstrated that our method can be used to perform patient-specific dose monitoring, enabling quality assurance on a level that was previously impractical. Using our system, we found that the median patient radiation doses were lower than those in previous reports. Even more valuable, however, is the distribution of individual patient doses that we obtained using our system. Studies where a patient received a radiation dose significantly higher than the average radiation dose, which currently may go undetected at most institutions, could be identified using our system and reviewed to determine the cause of the elevated dose. In addition, patient-specific dose monitoring permitted the assessment of variation in the delivered dose across an

institution, which enables technique optimization for specific x-ray tubes. Accordingly, problems that cause patient overdoses can now be corrected quickly, enhancing the overall quality of patient care.

Despite the evident utility of our patient-specific radiation dose monitoring program, there are limits to its application. We based our DCC tables on the phantom design of Cristy and Eckerman[16, 17]. This simplistic design fails to accurately represent all patient shapes and sizes. Further, the fact that patient heights and weights are not routinely recorded in the image file in most clinical environments also introduces uncertainty into our system. For these reasons, our patient-specific dose calculation provides only an estimate of the radiation dose received by an individual patient. Nevertheless, our patient-specific radiation dose estimates indicate the relative magnitude of patient doses and have the potential to significantly improve the quality of patient care.

2.5 Conclusions

To improve the quality assurance program in digital radiography, we developed a method for calculating patient-specific radiation dose from DR examinations. We generated DCC tables for all clinically relevant energy spectra based on kVp and total filtration values. To enable the use of these DCC tables with information available during normal clinical practice, we developed a method that uses the HVL to determine

total filtration. Finally, we demonstrated how these DCC tables can be used clinically to calculate radiation doses in chest radiography examinations.

3. Automated patient-specific CT dose monitoring system: assessing variability in CT dose

3.1 Background

Computed tomography (CT) was first introduced clinically during the 1970s. Since then, the number of CT scans performed annually has burgeoned to over 62 million[22]. This increased use of CT has greatly increased radiation exposure in the United States, and it is estimated that CT radiation is currently responsible for roughly 25% of the collective radiation dose to the United States population[1]. Further, the exposure of the patient population is expected to further expand in upcoming years due to the adaptation of CT for use in screening procedures[23].

CT necessarily delivers a higher radiation dose than other common imaging procedures because it requires hundreds of angular projections to generate 3D images. Therefore, repeated or unnecessary exposures can easily subject patients to excessive radiation doses. While media outlets have highlighted recent cases of severe overdose[2], even slight overdoses are thought to increase the risk of developing cancer and should be avoided[24]. Therefore, it is necessary to ensure that all patients receive a radiation dose from CT that is as low as reasonably achievable (ALARA).

Despite efforts to keep radiation doses as low as possible, however, there is a great deal of variability in the dose delivered to patients during CT scans[6, 7, 25, 26]. While this variability suggests that some patients may receive too high a radiation dose from CT scans, little actual data exist regarding the doses patients receive during

scanning. It is not current practice to record patient-specific radiation doses for all CT scans, and there are currently no methods in place for standardizing radiation dose within a single institution. Current efforts targeted toward benchmarking doses at individual institutions against national trends fall short of these goals.

To address this issue, we developed an automated patient-specific CT dose monitoring system to assess variability in CT dose to individual patients. Here, we describe this much-needed tool along with evidence demonstrating that it facilitates quality assurance as well as standardization of CT protocols.

3.2 Methods

3.2.1 Dose calculation

CT image data were sent from the picture archiving and communication system (PACS) to a secure dosimetry server, where Digital Image and Communication in Medicine (DICOM) routing software isolated CT dose reports. The standard CT dose report, shown in Figure 11, consists of a DICOM image file containing the CT dose index (CTDI), dose length product (DLP), and size of the CTDI phantom (either 16 cm or 32 cm). Additionally, the DICOM headers contain patient demographic information as well as examination parameters associated with the study.

Optical character recognition (OCR) was used to extract dose-relevant data from the dose report image files. An OCR algorithm segmented the dose reports into lines, words, and characters. Each character was compared to a dictionary file through 2D-

correlation analysis to translate the image file into text. The text file was searched in order to determine the phantom size and total exam DLP. The DICOM headers provided additional study information, including the study description, protocol, patient age, and patient gender. This information was stored in a dosimetry database for further processing.

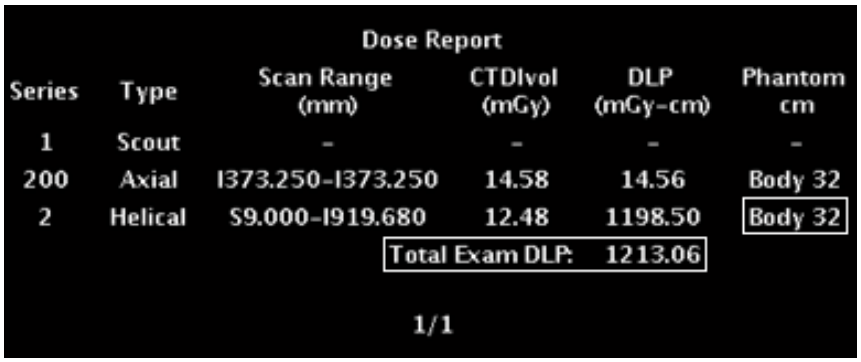

Dose Report

Series	Type	Scan Range (mm)	CTDIvol (mGy)	DLP (mGy-cm)	Phantom cm
1	Scout	-	-	-	-
200	Axial	I373.250-I373.250	14.58	14.56	Body 32
2	Helical	S9.000-I919.680	12.48	1198.50	Body 32
			Total Exam DLP:	1213.06	

1/1

Figure 11: Dose report image for CT.

Effective dose was calculated by multiplying the DLP by an age- and protocol-specific conversion coefficient (k-factor)[27]. Adult[28] and pediatric[29] k-factors were taken from previously conducted Monte Carlo simulations. Due to a lack of standardization in nomenclature, however, individual protocols did not correspond directly to specific k-factors. Instead, a key word search of the study description and protocol name was performed to determine the appropriate k-factor for each study. In cases where the key word search returned multiple k-factors, the highest value was chosen.

Table 3: k-factors used for CT dose calculation.

	Age				
Region	0	1	5	10	Adults
C/A/P					0.015
CHEST	0.057	0.038	0.026	0.019	0.020
A/P					0.015
ABD	0.05	0.031	0.021	0.015	0.018
PELVIS	0.049	0.031	0.021	0.015	0.010
ADRENALS					0.020
LIVER					0.020
KIDNEYS					0.017
HEAD	0.013	0.008	0.005	0.004	0.002
NECK	0.023	0.015	0.01	0.007	0.005
OTHER	0.057	0.038	0.026	0.019	0.020
EXT					0.001

3.2.2 Data analysis

We collected data from over 6,500 CT studies from two institutions over a 5-week period; for anonymity, we will refer to these institutions as Institution A and Institution B. Three representative protocols (routine head (n=777), standard chest (n=662), and abdomen pelvis (n=449)) were selected for data analysis. To assist in data analysis, we developed a graphical user interface capable of generating custom filters to isolate specific CT studies. The filters facilitated our assessment of variability in patient doses on three different levels: within a single protocol, between scanner models, and across institutions.

3.2.2.1 Variability in patient dose within single protocols

To visualize the variation in patient dose for each representative protocol, we generated scatter plots of individual patient doses. Diagnostic reference levels (DRLs) are an accepted tool to identify high dose studies for investigative purposes[30]. We established two dose levels: a diagnostic reference level for comparison across institutions and a dose action level for investigative purposes. The 75th percentile was used for the reference level, whereas the action level was set at three times the median dose for each protocol. This method allowed for fluctuations in dose due to variability in patient size while still identifying studies in which patient doses considerably deviated from the median. Studies where the dose exceeded the action level were flagged for review to determine the cause of the elevated dose.

3.2.2.2 Variability in patient dose between scanner models

We assessed the variability between three scanner models (Lightspeed VCT, Lightspeed Pro 16, and Definition CT750 HD) for both the standard chest protocol and abdomen pelvis protocol at a single institution. We were unable to assess variability between scanner models for the routine head protocol because of an insufficient number of studies on multiple CT scanner models within a single institution. Bar graphs showing the median as well as the 25th and 75th percentile doses for each scanner model were used to visualize differences in patient dose. Since the patient dose distributions were not normal, a Kruskal-Wallis one-way analysis of variance was used to assess

variability in patient dose across scanner models; p-values less than 0.05 were considered statistically significant.

3.2.2.3 Variability in patient dose across institutions

Median dose values were calculated for the routine head, standard chest, and abdomen pelvis protocols at both institutions. A bar graph showing the median as well as the 25th and 75th percentile doses for representative protocols at each institution allowed visualization of differences in patient dose. Since the patient dose distributions were not normal, a Mann-Whitney rank-sum test was used to assess variability in patient dose across institutions for each protocol; p-values less than 0.05 were considered statistically significant.

3.2.3 Risk estimation

Currently, the most commonly employed method for calculating patient risk involves multiplying the effective dose by a conversion factor (e.g., four cases of cancer incidence/rem per 10,000 exposed). While this method provides a reasonable estimate of patient risk in some instances, however, it fails to account for the fact that the risk associated with radiation is age- and gender-specific. Therefore, we computed estimates of patient-specific lifetime attributable risk of cancer incidence (in terms of cases per 10,000 patients exposed) for male patients undergoing chest (n=259) and abdomen pelvis (n=112) examinations by multiplying the DLP by age- and gender-specific conversion coefficients (q-factors)[31]; risk estimates were not determined for the routine head

protocol due to the unavailability of conversion coefficients. The q-factors were derived from the tables of organ risk factors previously published in the BEIR VII report[24]. The results from this new method were compared to the risk estimates calculated using the effective dose methodology as well as risk estimates calculated assuming all patients to be 20 years old.

Table 4: q-factors used for CT risk estimation with male patients (in units of incidence per 10,000 patients exposed per mSv).

	Age			
Region	20	40	60	80
C/A/P	0.0014	0.0009	0.0006	0.0002
CHEST	0.0016	0.0010	0.0007	0.0002
A/P	0.0016	0.0011	0.0007	0.0002
ABD	0.0015	0.0010	0.0007	0.0002
PELVIS	0.0015	0.0010	0.0006	0.0002
ADRENALS	0.0019	0.0013	0.0008	0.0003
LIVER	0.0017	0.0011	0.0008	0.0002
KIDNEYS	0.0015	0.0010	0.0007	0.0002

3.3 Results

3.3.1 Variation in patient dose within individual protocols

We assessed variability in patient doses from the routine head, standard chest, and abdomen pelvis protocols. The reference level (75th percentile) for the routine head protocol was 2.56 mSv. The median patient dose for the routine head protocol was 1.96 mSv, and we used this value to establish an action level of 5.89 mSv. Three studies (1.36%) had patient doses that considerably exceeded the action level requiring further investigation (Figure 12). Review of these cases revealed that the elevated doses were

intentional and justified. The most common cause of dose elevation was multiple scans within a single study.

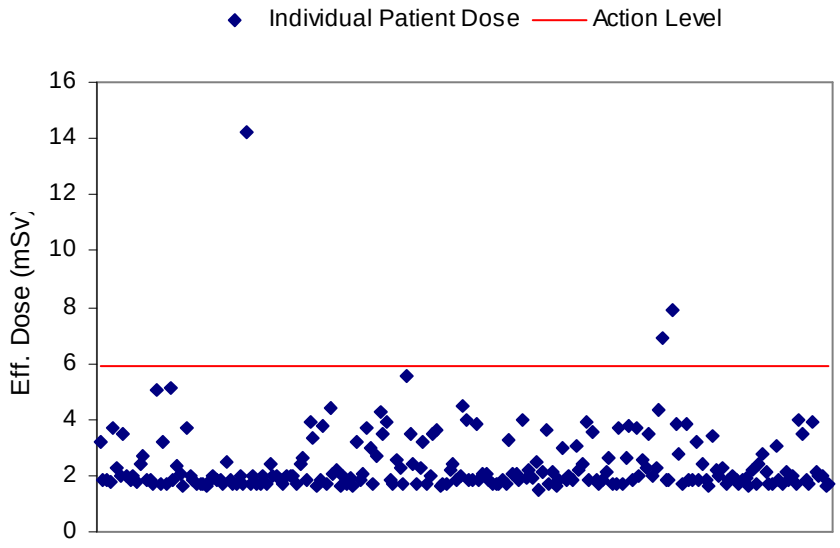

Figure 12: Scatter plot of patient doses for routine head CT scans.

The reference level (75th percentile) for the standard chest protocol was 8.84 mSv. The median patient dose and action level were 6.63 and 19.9 mSv, respectively. Due to the larger variation in patient size for this set of procedures, the distribution of patient doses was broader for the standard chest protocol than the routine head protocol. Despite this broader range, only two studies (0.64%) exceeded the action level and thus required further investigation (Figure 13). Review of these cases revealed that the most common reason for elevated dose was variation in patient size.

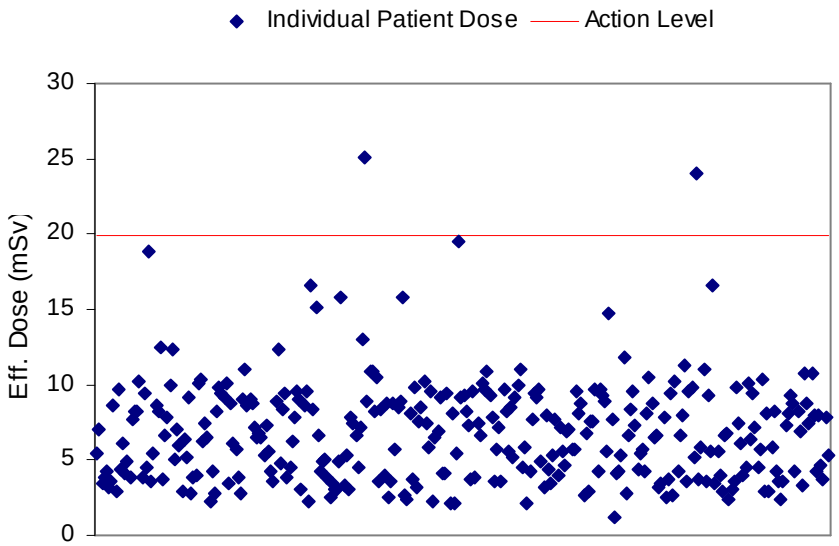

Figure 13: Scatter plot of patient doses for standard chest CT scans.

The reference level (75th percentile) for the abdomen pelvis protocol was 13.49 mSv. The median patient dose and action level were 10.50 and 31.5 mSv, respectively. Of the three protocols examined, the abdomen pelvis protocol exhibited the broadest distribution in patient doses. Four studies (2.48%) exceeded the action level and thus required further investigation (Figure 14). Review of these cases revealed that the most common cause of dose elevation was variation in patient size.

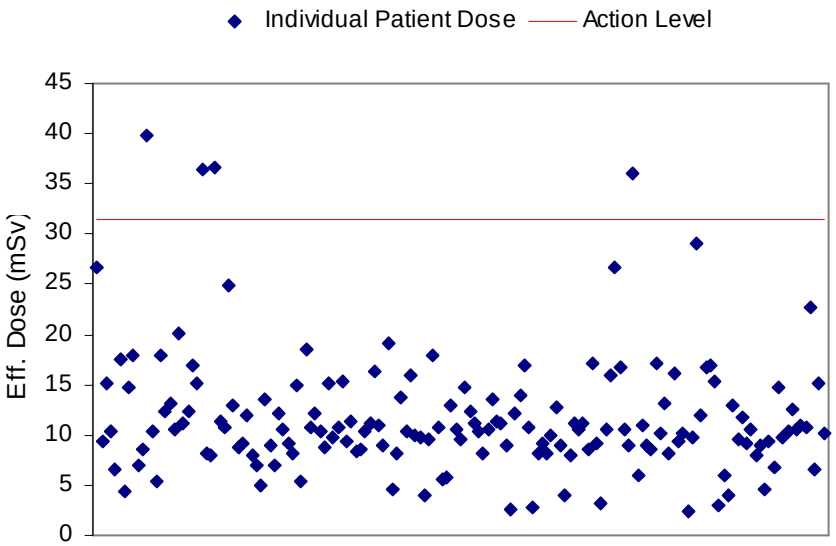

Figure 14: Scatter plot of patient doses for abdomen pelvis CT scans.

3.3.2 Variation in patient dose between scanner models

We next assessed variability in patient doses between scanner models at a single institution for the standard chest and abdomen pelvis protocols. Slight variation in patient dose existed across scanner models for the standard chest protocol (Figure 15). The median doses for studies conducted on the Lightspeed Pro16 were nearly identical to those conducted on the Lightspeed VCT. Interestingly, however, the median patient dose for the Definition CT750 HD was 22% lower than that for the Lightspeed VCT and Lightspeed Pro16. This reduction in patient dose arises primarily due to the use of iterative reconstruction algorithms by the Definition CT750 HD model. Due to the inherent variability in patient doses for this protocol, however, differences in patient dose between the three scanner models were not statistically significant ($p = 0.0876$).

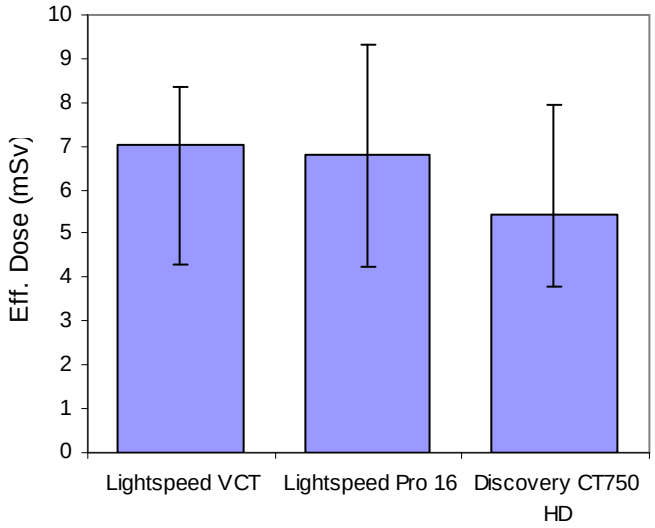

Figure 15: Patient doses on multiple CT scanner models for standard chest protocols.

We conducted a similar analysis of dose between scanner models for the abdomen pelvis protocol (Figure 16). Compared to the Lightspeed VCT, the median patient dose for studies conducted on the Lightspeed Pro16 and Definition CT750 HD were 13% and 42% lower, respectively. Analogous to our observations for the standard chest protocol, we again noted that the Definition CT750 HD model produced the lowest median patient dose for this scanning protocol. Although we observed even greater variation in the median patient dose for the abdomen pelvis than standard chest protocol, this difference in median dose was statistically significant ($p = 0.0067$).

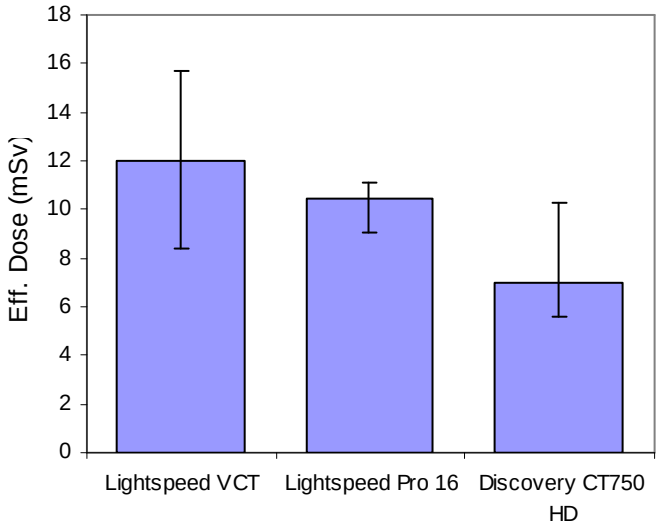

Figure 16: Patient doses on multiple CT scanner models for abdomen pelvis protocols.

3.3.3 Variation in patient dose across institutions

To assess variability in patient doses across institutions, we compared median patient doses from the routine head, standard chest, and abdomen pelvis protocols at both institutions. Compared to Institution A, the median patient dose at Institution B was elevated by 25%, 68%, and 63% for the routine head, standard chest, and abdomen pelvis protocols, respectively (Figure 17). For the all three protocols, this difference in patient dose across institutions was statistically significant ($p < 0.0001$ for all three protocols).

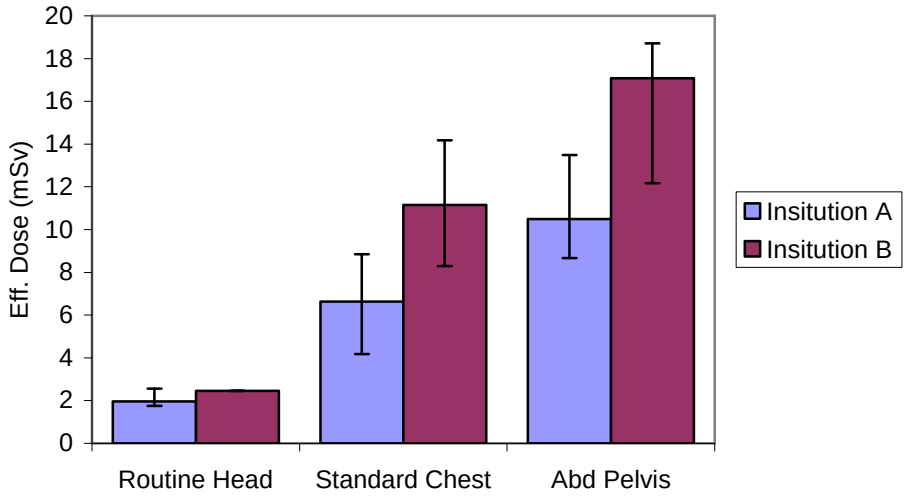

Figure 17: Patient doses for representative protocols between two institutions.

3.3.4 Risk estimation

We compared the patient risk index values calculated using actual patient ages to those calculated assuming a universal patient age of 20 years. For the chest protocol, average risk estimates decreased 2.7-fold (from 6.08 to 2.26 cases per 10,000 exposed) when patient ages were taken into account. For the abdomen pelvis protocol, average risk estimates decreased by 2.0-fold (from 13.83 to 6.85) when patient ages were taken into account.

Next, we compared the patient risk index values calculated using actual patient ages to those calculated using the effective dose methodology. The effective dose methodology yielded average patient risk estimates similar to those calculated using actual patient ages, with differences of 29% and 26% for the chest and abdomen pelvis protocols, respectively. However, the distribution of risk estimates was skewed

according to patient age. The effective dose method underestimated risk for patients younger than 40 years, whereas it overestimated risk for patients older than 60 years (Figures 19 and 20).

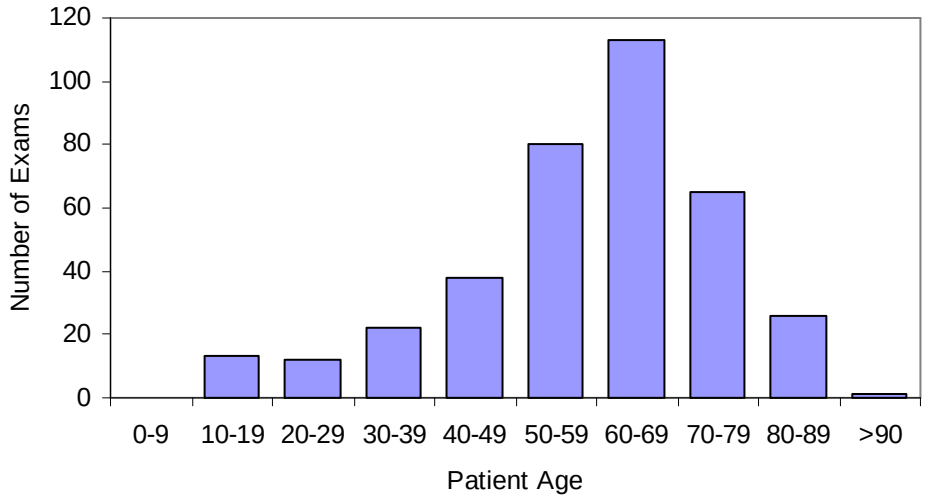

Figure 18: Age distribution for male patients undergoing chest and abdomen pelvis CT examinations.

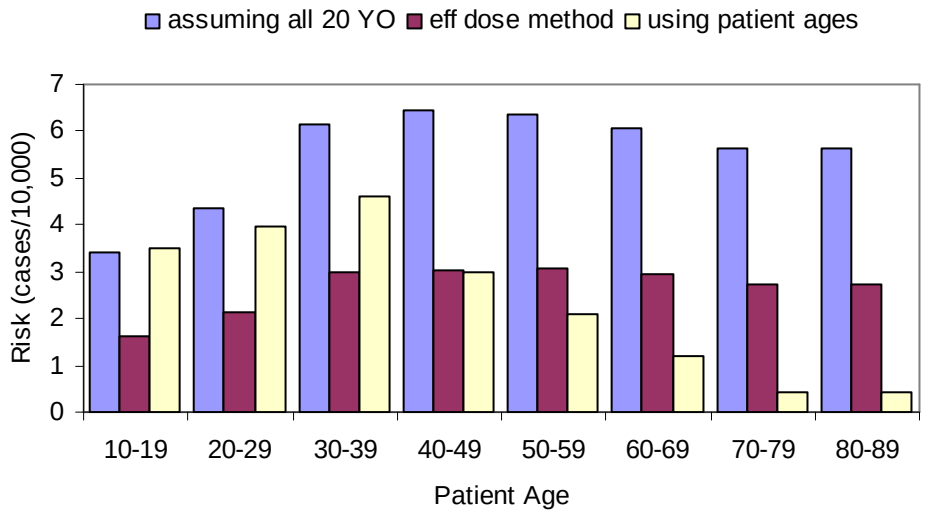

Figure 19: Risk estimates for male chest examinations.

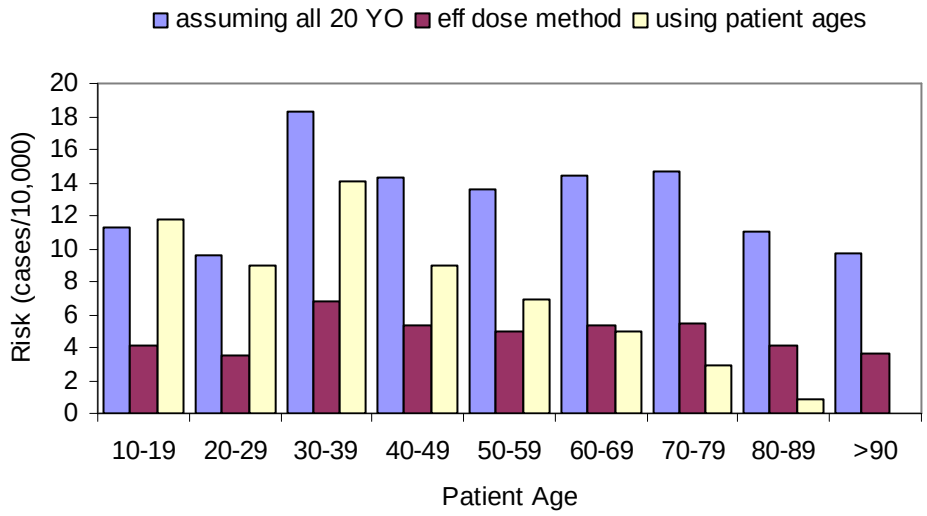

Figure 20: Risk estimates for male abdomen pelvis examinations.

3.4 Discussion

Our automated patient-specific dose monitoring system allows CT quality assurance and standardization on a level that was previously impractical. Using this system, we analyzed variability in individual patient dose within three representative scanning protocols, between three scanner models, and across three institutions. We implemented reference and action levels for patient doses and used these values to improve both the quality and consistency of patient care.

3.4.1 Variation in patient dose within single protocols

When we examined patient doses from the routine head, standard chest, and abdomen pelvis CT protocols, we observed high-dose outliers for all three protocols. In most cases, these outlying data points corresponded to studies where the increased dose was necessary and intentional. However, there were a few instances where further

review determined that patient dose could have been reduced during imaging. The use of our DRLs helped to identify and correct situations that led to elevated dose in these cases.

We recognize that there is a need for DRL standardization in the medical community. While others have used a certain percentile as an action level[6], this solution did not seem appropriate for a data set as large as ours (n= 1888). Additionally, percentile-based DRLs necessarily flag a given number of studies without considering the deviation within a distribution of patient doses. We have maintained the 75th percentile as a reference level; however, we have introduced an alternative action level that better reflects an acceptable amount of deviation in patient dose. Since the distribution of patient doses is not normal, isolating outliers using statistical analysis presents a difficult task. Our solution of using a cutoff three times the median dose offers a simple, easily adapted method that allows for variability in patient size while still ensuring that all patients receive comparable doses.

3.4.2 Variation in patient dose between scanner models

Data on the variations in patient dose across scanner models impact clinical practice in three ways: it indicates whether protocols are optimized for specific scanner models, it influences decisions about which scanners are used for which protocols, and it influences future purchases in the department. Using our dose monitoring system, we observed slight variation in patient doses between the Lightspeed VCT, Lightspeed Pro

16, and Definition CT750 HD scanner models. The reduced patient dose detected for the Definition CT750 HD was expected. This scanner employs iterative reconstruction algorithms, which require lower tube currents than other algorithms to achieve acceptable image quality. It is therefore not surprising that subjecting patients to scans with lower tube currents results in a reduction in patient dose.

3.4.3 Variation in patient dose across institutions

When comparing patient doses at different institutions, patients at Institution B received consistently higher radiation doses than did patients at Institution A. Determining the significance and causes of this trend is complicated by many factors, including differences in patient demographics, diagnostic focus, and protocol design between institutions. Nevertheless, the trend suggests there is an opportunity to reduce the radiation dose delivered to patients at Institution B. Accordingly, these data were presented to the hospital staff at Institution B to help them make informed decisions that will optimize the quality of the care they provide.

3.4.4 Risk estimation

Inclusion of patient age and gender significantly improved estimates of patient risk leading to an overall decrease in average patient risk estimates. Utilizing patient age and gender to inform our estimates also allowed us to identify and reevaluate studies for which risk estimates were not strictly correlated with patient dose. This reevaluation altered our assessment of which studies were associated with the highest

patient risk. Therefore, it is imperative to monitor patient-specific radiation risk, taking into account patient age and gender, in addition to generic radiation dose quantities such as effective dose.

3.4.5 Limitations

Despite its evident utility, we recognize that our automated patient-specific dose monitoring system for CT has limitations. First, this system relies on the DLP to calculate the effective dose for each study, and previous work has demonstrated that this method fails to account for differences in patient demographics and size[32]. Further, the DLP methodology has lagged behind the rapid advances in CT technology[33]. Nevertheless, currently the use of DLP remains the quickest, easiest, and most commonly used method to calculate patient dose. Until a better method is developed, therefore, we will continue to use the DLP for CT dose calculations while maintaining awareness of its biases.

Additionally, while recent work has improved the accuracy of dose conversion coefficients by using data on patient size[21], patient height and weight were not readily available in our studies. Given the fact that dose conversion coefficients can vary by as much as 32% between patients of different size, we are aware that this simplification biases the doses calculated in this study[31]. Nevertheless, this bias is most significant for large patients, for whom the true dose conversion coefficient is lower than the estimated value. Because this simplification results in an overestimation of patient dose,

therefore, we believe that it does not significantly impair our ability to achieve our primary aim of detecting high-dose cases in the patient population.

Finally, we acknowledge that uncertainties in patient-specific dose monitoring make this system ill-suited for use with individual patients. Indeed, we propose that our system is primarily designed as a tool to assess patient dose across large populations for the improvement of clinical practice. Our system allows data analysis that is otherwise impossible, and it permits accurate visualization of the variability in patient doses as well as identification of patients whose dose deviates significantly from the median. Therefore, our system offers a powerful tool for the standardization and optimization of CT protocols that is capable of quickly and efficiently integrating dose-relevant data from a large number of studies.

3.5 Conclusions

We developed an automated patient-specific dose monitoring system for CT. With this system, we were able to assess variability in patient dose within individual protocols, between scanner models, and across institutions. Further, we established a method to define DRLs that allows for variation in patient size when considering high volumes of CT studies. We show here that our system detected slight variability in patient dose between scanners and significant variability in dose across institutions, indicating the opportunity to reduce patient radiation dose. This new dose monitoring

system offers a unique tool for improving quality assurance and standardization both within and across institutions

References

1. National Council on Radiation Protection and Measurements. and National Council on Radiation Protection and Measurements. Scientific Committee 6-2 on Radiation Exposure of the U.S. Population., *Ionizing radiation exposure of the population of the United States*. NCRP report. 2009, Bethesda, Md.: National Council on Radiation Protection and Measurements. xv, 387 p.

2. Bogdanich, W. (2009) *Radiation Overdoses Point Up Dangers of CT Scans* New York Times.

3. Spelic, D., *Preliminary results of the 2001 nationwide evaluation of X-ray Trends (NEXT) survey of adult chest radiography.* Medical Physics, 2002. **29**(6): p. 1373-1373.

4. Wang, S., *The "Dose Index Tracker": An Automated Database of Patient Radiation Dose Records for Quality Monitoring*. 2010.

5. Cook, T. *Radiance*. 2010; Available from: http://www.pennradiology.com/radiance/index.php.

6. Seeram, E. and P.C. Brennan, *Diagnostic reference levels in radiology.* Radiol Technol, 2006. **77**(5): p. 373-84; quiz 385-7.

7. Cody, D.D., et al., *Normalized CT Dose Index of the CT Scanners Used in the National Lung Screening Trial.* American Journal of Roentgenology, 2010. **194**(6): p. 1539-1546.

8. Stern, S.H., et al., *Nationwide evaluation of x-ray trends (NEXT) 2000-2001 survey of patient radiation exposure from computed tomographic (CT) examinations in the United States.* Radiology, 2001. **221**: p. 161-161.

9. United Nations. Scientific Committee on the Effects of Atomic Radiation., *Sources and effects of ionizing radiation : United Nations Scientific Committee on the Effects of Atomic Radiation : UNSCEAR 2000 report to the General Assembly, with scientific annexes*. 2000, New York: United Nations.

10. Hummel, R.H., R.L. Wesenberg, and G.M. Amundson, *A Computerized X-Ray Dose-Monitoring System.* Radiology, 1985. **156**(1): p. 231-234.

11. Hart, D., *Estimation of effective dose in diagnostic radiology from entrance surface dose and dose-area product measurements.* 1994.

12. Jones, D., *Organ doses from medical x-ray examinations calculated using Monte Carlo techniques.* 1985.

13. Rosentein, *Organ Doses in Diagnostic Radiology.* Bureau of Radiologic Health, 1976.

14. Shrimpton, P.C., *Calculation of patient skin dose from diagnostic X-ray procedures.* Br J Radiol, 1985. **58**(689): p. 483-5.

15. Tapiovaara, M.L., M. Servomaa, A., *PCXMC: A PC_based Monte Carlo program for calculating patient doses in medical x-ray examinations.* Helsinki: Finish Centre for Radiation and Nuclear Safety, 1997.

16. Cristy, M., *Mathematical phantoms representing children of various ages for use in estimates of internal dose.* 1980.

17. Eckerman, K.F., *The ORNL mathematical phantom series.* 1996.

18. Schmidt, P.W.E., et al., *Conversion factors for the estimation of effective dose in paediatric cardiac angiography.* Physics in Medicine and Biology, 2000. **45**(10): p. 3095-3107.

19. Schultz, F.W., et al., *Monte Carlo calculations for assessment of radiation dose to patients with congenital heart defects and to staff during cardiac catheterizations.* British Journal of Radiology, 2003. **76**(909): p. 638-647.

20. Flynn, M.J., *Xspect 3.5*. 2004.

21. Li, X., et al., *Patient-specific radiation dose and cancer risk estimation in CT: part I. development and validation of a Monte Carlo program.* Med Phys, 2011. **38**(1): p. 397-407.

22. Brenner, D.J. and E.J. Hall, *Computed tomography--an increasing source of radiation exposure.* N Engl J Med, 2007. **357**(22): p. 2277-84.

23. *National Lung Screening Trial (NLST).* Geriatrics, 2002. **57**(11): p. 16-16.

24. National Research Council (U.S.). Committee to Assess Health Risks from Exposure to Low Level of Ionizing Radiation., *Health risks from exposure to low levels of ionizing radiation : BEIR VII Phase 2*. Beir. 2006, Washington, D.C.: National Academies Press. xvi, 406 p.

25. Jaffe, T.A., et al., *Radiation dose for body CT protocols: variability of scanners at one institution.* AJR Am J Roentgenol, 2009. **193**(4): p. 1141-7.

26. Jaffe, T.A., et al., *Radiation dose for routine clinical adult brain CT: Variability on different scanners at one institution.* AJR Am J Roentgenol, 2010. **195**(2): p. 433-8.

27. Huda, W., K.M. Ogden, and M.R. Khorasani, *Converting dose-length product to effective dose at CT.* Radiology, 2008. **248**(3): p. 995-1003.

28. Li, X., et al., *Patient-specific radiation dose and cancer risk estimation in CT: part II. Application to patients.* Med Phys, 2011. **38**(1): p. 408-19.

29. Shrimpton, P.C., et al., *Effective dose and dose-length product in CT.* Radiology, 2009. **250**(2): p. 604-5.

30. *ICRP Publication 73. Radiological Protection and Safety in Medicine.* Annals of the ICRP, 1996.

31. Li, X., *The Feasibility of Universal DLP-to-Risk Conversion Coefficients for Body CT Protocols.* Abstract submitted to the SPIE conference, 2011.

32. Brenner, D.J., *Is it time to retire the CTDI for CT quality assurance and dose optimization?* Med Phys, 2005. **32**(10): p. 3225-6.

33. Dixon, R.L., *A new look at CT dose measurement: beyond CTDI.* Med Phys, 2003. **30**(6): p. 1272-80.